DISTRIBUTION STATEMENT A. Approved for public release; distribution is unlimited.

Large-Eddy Simulations of Baroclinic Instability and Turbulent Mixing

Eric D. Skyllingstad
College of Oceanic and Atmospheric Sciences, Oregon State University
104 COAS Admin. Bldg., Corvallis, OR 97331
Phone: (541) 737-5697 Fax: (541) 737-2540 Email: skylling@coas.oregonstate.edu

Roger M. Samelson
College of Oceanic and Atmospheric Sciences, Oregon State University
104 COAS Admin. Bldg., Corvallis, OR 97331
Phone: (541) 737-4752 Fax: (541) 737-2064 Email: rsamelson@coas.oregonstate.edu

Award Number: N00014-09-1-0268

LONG-TERM GOAL

The long-term goal of this project is to improve our ability to understand, model and predict lateral mixing and the associated submesoscale physical structure and processes in the upper and interior ocean.

OBJECTIVES

The main objective of this project is to examine the interaction between baroclinic, mesoscale eddies and turbulence using a large-eddy simulation (LES) model. Cases will focus on strong, baroclinic waves that form in the mixed layer along surface fronts with scales of a few km, and on mesoscale eddies that are imbedded within larger scale frontal regions. Our goal is to quantify, understand, and ultimately parameterize the physical processes that lead to lateral mixing. Simulations will help guide field experiments planned as part of the Lateral Mixing DRI, and provide a tool for understanding observations in the analysis phase of the project.

APPROACH

High-resolution simulations of baroclinic instability and the interaction of mesoscale flow with turbulent mixing are conducted and analyzed using a large-eddy simulation model. Our analysis centers on quantifying and understanding the mechanisms by which small-scale turbulent structure develops on the mesoscale field, the physical processes and balances that control lateral mixing of fluid properties across the unstable front, and the transition from strongly horizontal, geostrophic motion on the mesoscale to three-dimensional, quasi-isotropic, non-hydrostatic motion on turbulent scales.

WORK COMPLETED

Research during the second year of this project has focused on analyzing the effects of submesoscale baroclinic instability on lateral mixing and the effects of wind and wave forcing on these instabilities. The primary focus of this effort is to understand how the wind forced mixed layer interacts with baroclinic instability in forcing frontal slumping and cross frontal mixing.

RESULTS

Geostrophic Upper-Ocean Front

Frontal simulations were initialized using density gradients outlined Fox-Kemper et al. (2008), with the cross-frontal density structure set using,

$$b = N^2(z + H_o) + \frac{L_f M_f^2}{2} \tanh\left[\frac{2(y - y_o)}{L_f}\right] + b_o$$

where $b = -g\rho/\rho_o$, $N = \sqrt{\frac{-g}{\rho_o}\frac{\partial \rho}{\partial z}}$, z is the depth, H_o is the mixed layer depth, L_f is the frontal width, M_f is horizontal buoyancy gradient proportional to the Coriolis term f, y is the lateral direction, and b_o is the background buoyancy. Two values for the buoyancy frequency, N, were imposed representing the mixed layer and underlying pycnocline. Parameter selection for this initialization was set according to the theoretically fastest growing baroclinic mode with wavelength defined by,

$$L_s = \frac{2\pi U}{|f|}\sqrt{\frac{1 + Ri}{5/2}}; \quad \text{where} \quad Ri = \frac{N^2 f^2}{M^4}, \quad U = \frac{M^2 H}{f}.$$

Here we selected a temperature gradient of 0.1 ^{o}C over a distance of L_f = 600 m, which generated a baroclinic wavelength of about 5 km.

Simulations were conducted using a periodic domain with a rigid lid and flat bottom surface. Grid dimensions for the model were set to 3500 points in the cross frontal direction, 1920 points in the along frontal direction and 40 levels in the vertical. With a grid spacing set to 3 m, the resulting domain size was 10.5 km by 5.8 km horizontally with a depth of 120 m.

Vertical temperature in the model was set to a constant 17 ^{o}C between the surface and 80 m depth, with a constant temperature gradient thermocline of 0.023 ^{o}C/m below 80 m to the model lower boundary. We initialized a double front as shown in Figure 1a with a current structure set by assuming a thermal wind balance.

No Wind Forcing

We first present results from a basic case of frontal instability with no external forcing. Plots of the surface temperature and meridional velocity are presented in Figure 1 showing the development and evolution of a baroclinic wave on each front. Both fronts begin to buckle at around hour 78 with one major wave on each front. By hour 96, the wave on the left side front has amplified and is starting to eject a volume of cold fluid into the warm water region. On the right hand side front, the baroclinic wave develops a sharp cusp, with a smaller, detached cold eddy. Over time, the left side eddy forms a cold-core circulation with small perturbations that rotate around the central core. Overall, the frontal structure does not show significant cross frontal mixing except near the baroclinic eddy structures. In fact, many sections of the front sharpen over time in response to baroclinic instability, for example near x = 8000 m, y = 3000 m at hour 120. As the frontal gradients change, the meridional velocity follows suit in accordance with the changing thermal wind gradient. For example, the maximum southward velocity is located near the strong frontal interface noted above at hour 120.

Frontogenesis is a natural consequence of baroclinic instability as frontal boundaries are strained by wave-induced circulations. Frontogenesis accompanying upper-ocean submesoscale baroclinic

instability is generated by ageostrophic secondary circulations associated with large scale straining. Strong frontal velocity gradients develop small-scale instabilities that are more apparent when examining the flow with greater detail. Disturbances with scales of order 10-50 m are centered along the front in the region with highest horizontal shear.

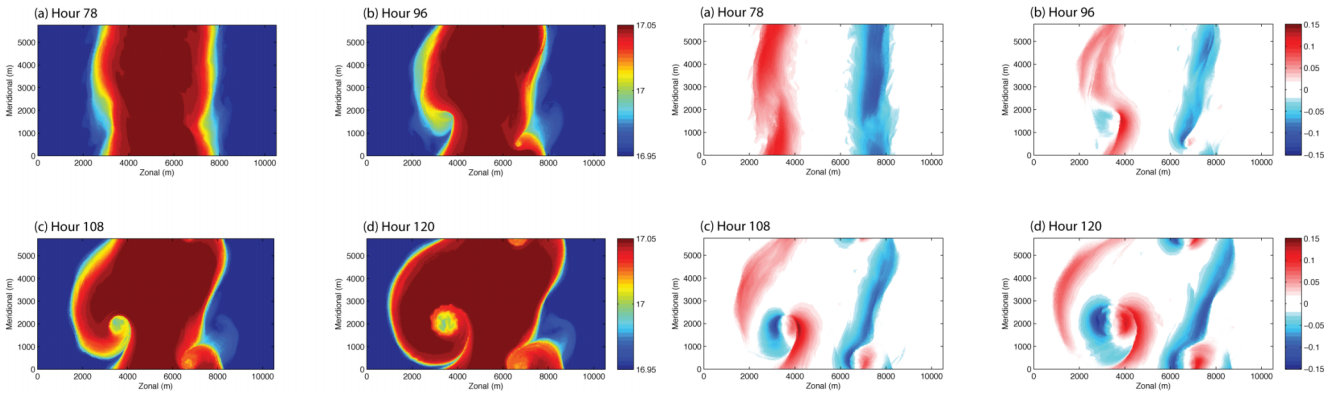

Figure 1. Horizontal sections of surface temperature (^{o}C, left side) and v component of velocity (m s^{-1}, right side) taken from (a) hour 78, (b) hour 96, (c) hour108, and (d) hour 120 for the Unforced case simulation.

Wind-Forced Case

Wind and wave forcing is applied in the model using a surface stress boundary condition and the Craik and Leibovich (1976) vortex force term, following previous studies of Langmuir circulation (see Skyllingstad and Denbo, 1995). Wind forcing is applied using Hour 60 initial conditions, which represents the flow just before the formation of instability waves. The wind stress amplitude is set to 0.1 N m^{-2}, and the Stokes-drift wave-forcing velocity profile is set using a monochromatic wave with 1-m amplitude and 30-m wavelength of 30 m.

Horizontal plots of the surface temperature from case W60 at three different times starting from the initial state are shown in Figure 2. The wind forcing for this case is northerly, i.e., directed toward negative y, and has a clear effect on the instabilities at both fronts. For the right-hand front near x = 7500 m, the wind is down-jet, i.e., directed with the frontal geostropic flow, so that Ekman transport is from cold to warm. This near-surface Ekman transport destabilizes the vertical water column, causing a more rapid spin-up of baroclinic eddies with shorter wavelengths, in comparison with the no-wind case (Figure 1). Two waves have developed by hour 96, which rapidly amplify and break down by Hour 108. Overall mixing with these disturbances is accelerated in comparison with the no-wind case, generating a wide gradient in temperature at the surface by hour 108 at the right-hand front.

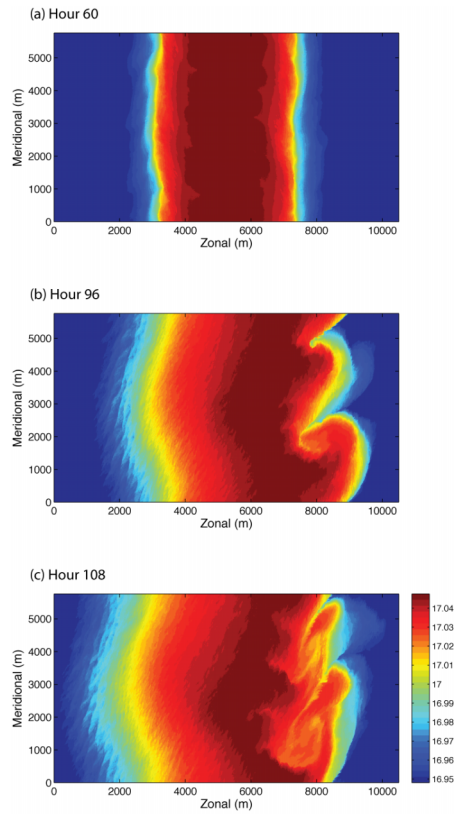

Figure 2. Surface temperature for case with northerly wind and waves.

Small Scale Structures

Small-scale coherent structures along the left-hand front are shown more clearly in Figure 3 for the northerly wind case initiated at hour 60. Horizontal sections over the front suggest that the horizontal temperature structure has a controlling effect on the scale of Langmuir circulation. Along the western side of the sub domain, vertical velocity (Figure 3b) displays small-scale features that are similar in form to typical Langmuir turbulence simulations as presented in Skyllingstad and Denbo (1995) or McWilliams et al. (1997). Temperatures in this region are relatively uniform in the vertical with mixed layer depths greater than 50 m.

On the eastern side of the domain, a banded temperature structure corresponding to temperature "ramps" is evident with vertical velocity aligned with horizontal temperature discontinuities. Vertical velocities associated with these circulations are between -0.04 and 0.04 m s^{-1}, which is nearly a factor of 10 greater than the frontal induced circulations indicated in the no wind case above. The ramp-like structure noted with this case is very similar to in situ autonomous underwater observations reported in Thorpe et al. (2003) showing a pattern of gradually increasing temperature followed by an abrupt decrease. Thorpe et al. (2003) suggest that Langmuir circulation generate these ramps, but do not implicate a background horizontal gradient in their analysis. Nevertheless, their temperature plot (figure 10, Thorpe et al. 2003) shows an overall temperature change across the ramps in accordance with the presence of a background horizontal gradient.

Abrupt changes in the temperature structure and accompanying vertical velocity circulations are similar to the secondary circulation that is produced during frontogenesis. Increased negative surface velocities (figure 3d) associated with coherent Langmuir circulations generate strong convergence that reinforces surface frontal features (for example, near x = 1500 m). This process is similar to modeling results presented in Thomas and Lee (2005), but on a smaller scale. In Thomas and Lee (2005), a series of fronts with separations of about 4 km are produced by down-front wind forcing and an ageostrophic secondary circulation. Here, coherent circulations generated by Langmuir forcing act in a similar way as the secondary circulation, providing convergence that generates ramp-like frontal zones on scales of 200 m versus the roughly 4000 m scales in Thomas and Lee (2005).

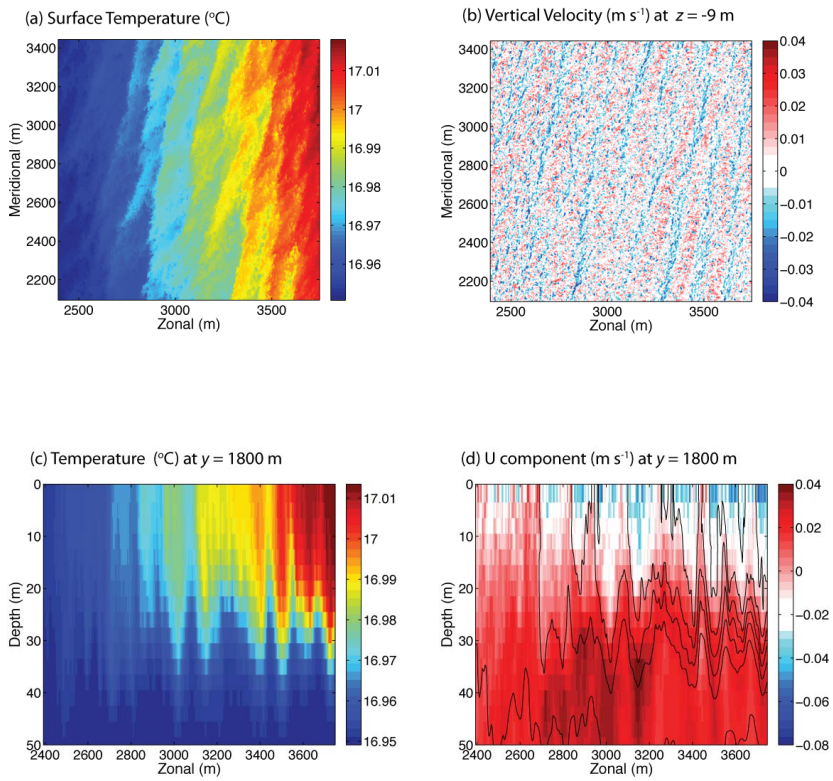

Figure 3. Horizontal plots of (a) surface temperature and (b) vertical velocity, w, at 9 m depth, along with cross sections of (c) temperature and (d) zonal velocity, u, taken from hour 84 of Case W60. Vertical cross sections are averaged meridionally over 10 grid points centered on y = 1800 m.

One of the main goals of this study centered on determining how baroclinic eddies transfer energy to turbulence scales that feed into the inertial subrange. We found that for cases without wind and wave forcing, horizontal and vertical shear generated in narrow frontal zones can develop weak three-dimensional turbulence that are directly linked to the larger scale baroclinic waves. Disturbances with scales between the baroclinic eddies and the small-scale turbulence are less organized, and do not appear to act as a conduit of energy between the baroclinic and turbulent scales.

Adding wind and wave forcing to the simulations produces a strong response in the formation and evolution of the frontal instabilities, depending on the direction of the wind relative to the initial front orientation and the associated surface geostrophic flow, in agreement with Thomas and Lee (2005).

For winds opposing the frontal geostrophic currents (up-jet winds), Ekman transport prevents the formation of instabilities, and the frontal zone is rapidly mixed through vertical and horizontal transport by Langmuir circulation and shear-induced turbulence. Winds aligned with the geostrophic currents (down-jet winds) enhance the formation of instabilities and reduce their horizontal scale. Lateral mixing for the down-jet winds is more rapid than for the unforced case, and results in a much more diffuse frontal zone. We find that in the down-jet wind case, a much stronger cascade of energy following a standard -5/3 slope is produced between the baroclinic and turbulent scales, in comparison with the unforced case.

REFERENCES

Craik, A. D. D., and S. Leibovich, 1976. A rational model for Langmuir circulations. *J. Fluid Mech.*, 73, 401-426.

Fox-Kemper, B., R. Ferrari, and R. Hallberg, 2008. Parameterization of mixed layer eddies. I: Theory and diagnosis. *J. Phys. Oceanogr.*, 38, 1145-1165.

McWilliams, J. C., P. P. Sullivan, and C.-H. Moeng, 1997. Langmuir turbulence in the ocean. *J. Fluid Mech.*, 334, 1-30.

Skyllingstad, E.D. and D. W. Denbo, 1995. An ocean large-eddy simulation of Langmuir circulations and convection in the surface mixed layer. *J. Geophys. Res.*, 100, 8501-8522.

Thomas, L. N., and C. M. Lee, 2005. Intensification of ocean fronts by down-front winds. *J. Phys. Oceanogr.*, 35, 1086-1102.

Thorpe, S. A., T. R. Osborn, J. F. E. Jackson, A. J. Hall, and R. G. Lueck, 2003. Measurements of turbulence in the upper-ocean mixing layer using autosub. *J. Phys. Oceanogr.*, 33, 122-145.